

# Multi-Messenger Windows on the Universe: detecting precursor emission to compacts' mergers

Maxim Lyutikov

Department of Physics, Purdue University,  
525 Northwestern Avenue, West Lafayette, IN 47907-2036

## ABSTRACT

We provide an overview of various mechanisms, and corresponding powers, of precursor emission to compacts' mergers to be detected by LIGO-Virgo-KAGRA (LVK) collaboration. Expected peak powers,  $\leq 10^{43}$  erg s $^{-1}$ , are not sufficiently high to be detected by all-sky high-energy satellites (unless beamed). The best chance is the detection of possible coherent radio emission, producing observable signals up to  $\sim$  Jansky of flux density. Low-frequency phased array telescopes like LOFAR, the MWA and DSA-2000 are best suited due to their large instantaneous sky coverage. Time-wise, in addition to LIGO early warning alerts up to a minute before the merger, the dispersive delay at lower frequencies of  $\sim 300$  MHz can be of the order of minutes. Optical detections are the most challenging.

## Contents

<b>1</b>	<b>Introduction: expected EM power of mergers</b>	<b>2</b>
<b>2</b>	<b>Magnetospheric interaction of merging neutron stars</b>	<b>3</b>
2.1	Estimates of the average power . . . . .	3
2.2	The merger of two NSs is necessarily electromagnetically dissipative . . . . .	3
2.3	Production of flares in DNS mergers . . . . .	4
2.4	Magnetic field evolution during NS to BH collapse . . . . .	8
<b>3</b>	<b>Magnetospheric interaction in BH-NS mergers</b>	<b>10</b>
<b>4</b>	<b>Observation strategy</b>	<b>12</b>
4.1	Best chance: low frequency radio . . . . .	13
4.2	High energy: beaming needed . . . . .	13
4.3	Optical . . . . .	14
<b>5</b>	<b>Supermassive BH-BH mergers and LISA precursors</b>	<b>14</b>

<b>6 In conclusion</b>	<b>15</b>
<b>7 Disclaimer and Acknowledgment</b>	<b>15</b>

### 1. Introduction: expected EM power of mergers

LIGO early warning alerts (Sachdev et al. 2020), [https://emfollow.docs.ligo.org/userguide/early\\_warning.html](https://emfollow.docs.ligo.org/userguide/early_warning.html) are expected to provide localization to  $\sim 300 - 1000$  square degrees up to a minute before merger. This opens a possibility of observing precursor electromagnetic emission to gravitational waves sources. Here we discuss the expected powers, modulation, and corresponding observing strategies.

Compacts' mergers (double neutron stars, DNS, neutron star-black hole, and double black holes) are expected to occur in old systems, with not much surrounding material. Thus, little pre-merger accretion power is expected (Foucart et al. 2018; Nakar 2020). Tidal disruption during active stages of mergers<sup>1</sup> will produce optically thick material that will likely blanket instantaneous radiation, see though §8. In addition, prospective sites of coherent radio emission - the likeliest detectable candidate, see below - will likely be polluted and radio emission switched off by the abundant tidally ejected material.

Observable radiation, if any, may still come from the electromagnetic interaction of merging stars. The underlying mechanism is the variant of unipolar induction operating in highly magnetized relativistic plasma self-produced by the merging companions. The basic estimate of EM power expected from a relativistic unipolar inductor (*e.g.*, Blandford 2002) is

$$L \sim \frac{c}{4\pi} (\Delta\Phi)^2 \quad (1)$$

where

$$(\Delta\Phi) \sim \beta DB \quad (2)$$

is the EMF drop for a conductor of size  $D$  moving in magnetic field  $B$  with velocity  $v = \beta c$ . The factor  $4\pi/c = 377$  Ohm is sometimes called the impedance of free space.

For rotating neutron stars, the potential drop  $\Delta\Phi$  is over the light cylinder:  $\Delta\Phi \sim B_{NS} R_{NS}^3 (\Omega_{NS}/c)^2$  (Goldreich and Julian 1969). For a linearly moving neutron star or black hole the potential drop  $\Delta\Phi$  is over the linear dimension of a conducting body (Goldreich and Lynden-Bell 1969; Lyutikov 2011a).

Next, we discuss various applications on the relation (1) to LVK and LISA sources: Keplerian motion of merging objects, neutron stars and black holes, as well as spinning magnetized neutron stars and black holes.

---

<sup>1</sup>For BH-NS mergers, a BH of mass  $\geq 5M_{\odot}$  will not tidally disrupt the NS.

## 2. Magnetospheric interaction of merging neutron stars

### 2.1. Estimates of the average power

The first basic application of the relation (1) is to a merger of an unmagnetized neutron star (so,  $D \sim R_{NS}$ ) moving with Keplerian velocity through the magnetospheres of the companion (Hansen and Lyutikov 2001), Fig. 1

$$L_{1NS} \sim \frac{B_{NS}^2 GM R_{NS}}{c} \left( \frac{R_{NS}}{r} \right)^7 = \begin{cases} 5 \times 10^{44} \text{ erg s}^{-1} \left( \frac{R_{NS}}{r} \right)^7 \\ 9 \times 10^{37} \text{ erg s}^{-1} \left( \frac{-t}{\text{sec}} \right)^{-7/4}, \end{cases} \quad (3)$$

where we used time to merger  $t$

$$-t = \frac{5}{256} \frac{c^5}{G^3} \frac{r^4}{M_1 M_2 (M_1 + M_2)} \quad (4)$$

is measured in seconds in Eq. (3). (For numerical estimates we assume surface fields of  $B_{NS} = 10^{12}$  G. Due to tidal distortions, the minimal time in (4) is  $\tau_0 \sim 10^{-3}$  sec (this is the peak of LVK), giving the peak power of

$$L_{peak} \sim 10^{43} \text{ erg s}^{-1}, \quad (5)$$

see (Hansen and Lyutikov 2001; Most and Philippov 2023).

Though the relation (1) appeals to induction - a non-dissipative process - in reality, the inductively created electric fields can have a component along the total magnetic field (gaps) and/or the electric field may exceed the value of the local magnetic field, see below.

Relations (1-5) are important basic estimates. The peak power - emitted within a millisecond, is not large, making it challenging to detect.

Another important point about detectability is the possible orbital modulation of the emission. If only one star is magnetized the emission is likely to be produced along the direction of the magnetic field at the location of the secondary; then, if the magnetic axis is misaligned with the orbital spin, this direction is modulated on the orbital period.

If both stars are magnetized, the effective size of “fractioning magnetospheres is the orbital separation,  $D \sim r$ . In this case, the power of  $R_{NS}/r$  in (3) is  $(R_{NS}/r)^5$  instead of 7 (Lyutikov 2019; Most and Philippov 2022). So, larger ramp-up power, approximately the same peak power.

For the double-magnetized case, the structure of the common magnetosphere of the non-rotating neutron stars is complicated, with gaps, but no  $E > B$  regions, Fig. 2. There is strong orbital variations for the case of misaligned magnetic moments.

### 2.2. The merger of two NSs is necessarily electromagnetically dissipative

The above discussion implicitly assumes that the emitted electromagnetic energy comes from the kinetic energy of Keplerian motion, but it does not address the question why and how the

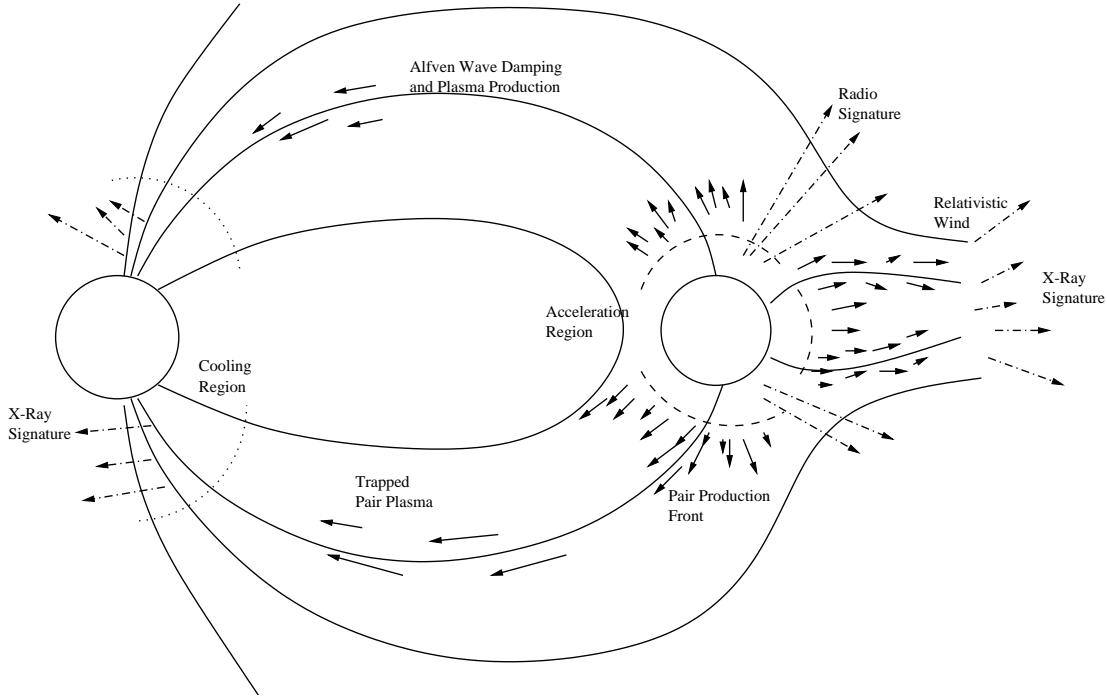


Fig. 1.— Schematic version of the energy extraction process. The motion of the companion through the magnetar field induces a plasma flow from the companion into the magnetosphere. The pressure of this flow will drive a relativistic wind in those regions where the flow moves into a regime of a weaker field, while the plasma remains trapped in the case when it flows into a stronger field regime. The hot pair plasma will ablate some baryons off the surface of the neutron star, providing a baryon-loaded sheath that regulates the cooling of the trapped plasma (after Hansen and Lyutikov 2001).

dissipation takes place. It turns out that *the electromagnetic interaction of merging neutron stars is necessarily dissipative* due to the effect of electromagnetic draping - the creation of dissipative regions near the companion (unmagnetized) star (Lyutikov 2023). The draping effect is well-known in space and astrophysical plasmas (Cairns 2004; Lyutikov 2006; Dursi and Pfrommer 2008). In the conventional non-relativistic MHD limit the creation of the magnetized layer (for super-Alfvénic motion) does not lead to dissipation, only a breakdown of the weak-field approximation in the draping layer.

### 2.3. Production of flares in DNS mergers

The above estimates of *average* power (3-5) are relatively small. Importantly, those estimates assume continuous dissipation. Possible production of flares - whereby energy is slowly stored and then suddenly released - may produce (orbital-modulated) flares. Indeed, a magnetic connection between merging magnetized neutron stars may lead to the production of a special configuration of interacting magnetospheres of merging neutron stars (Cherkis and Lyutikov 2021).

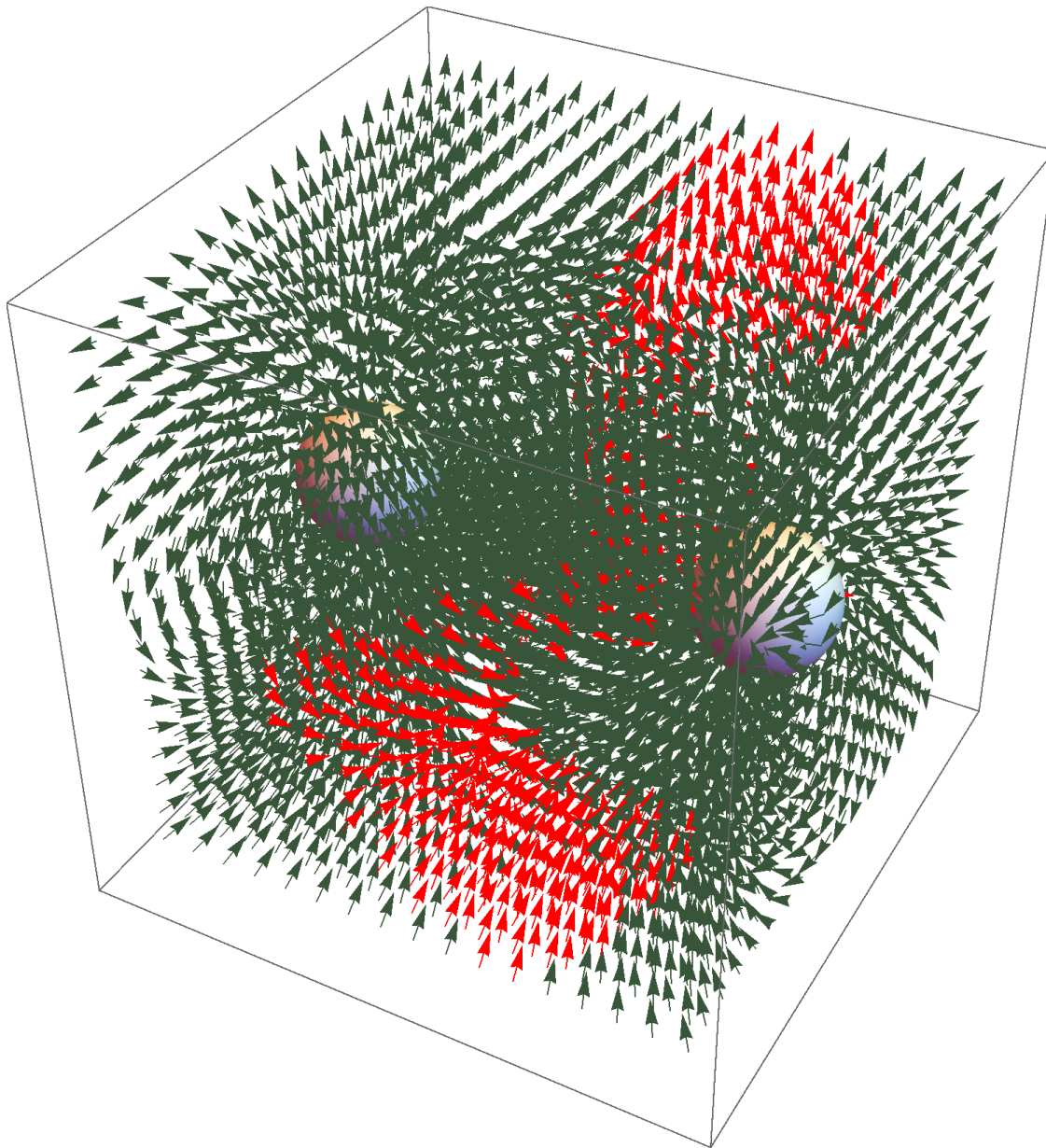


Fig. 2.— 3D rendering of the common magnetosphere of the interacting neutron stars, orthogonal dipoles. Highlighted in red are regions with high parallel electric field (Lytikov 2019).

In the case of interacting magnetospheres, there are special configurations when the stellar spins and the orbital motion nearly ‘compensate’ each other, leading to very *slow* overall winding of the coupled magnetic fields; slowly winding configurations allow gradual accumulation of magnetic energy, that is eventually released in a flare when the instability threshold is reached. This slow winding can be global and/or local. The conditions for the storage of magnetic energy sometimes become ambiguous near the topological bifurcation points; in certain cases, they also depend on the

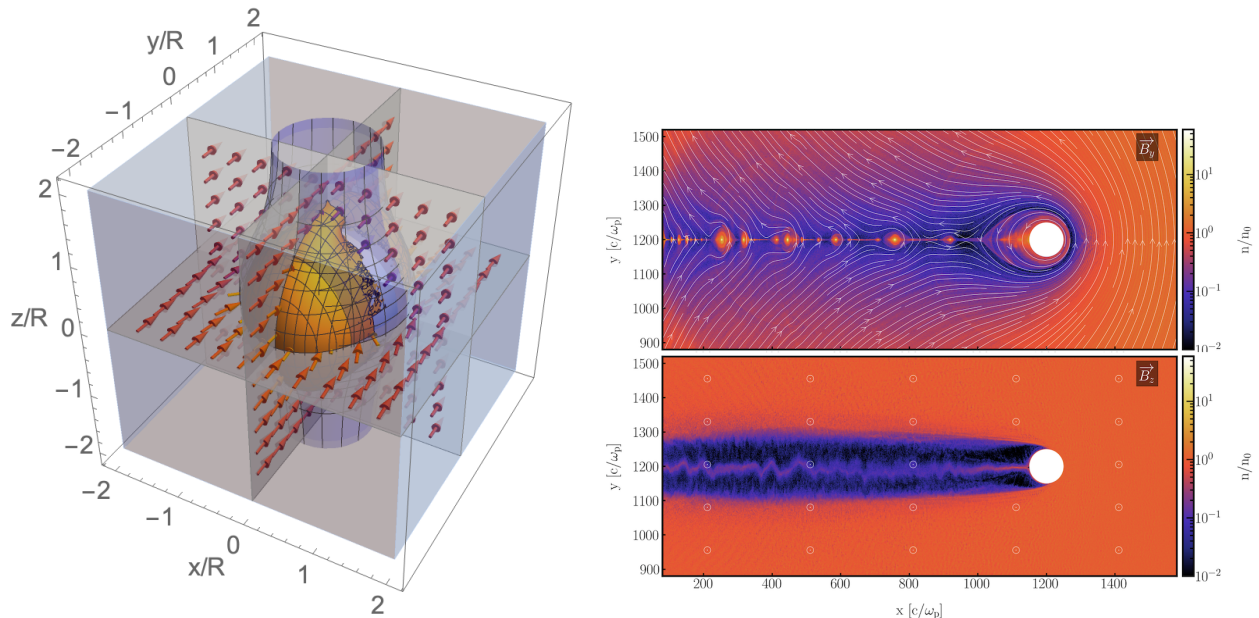


Fig. 3.— Left panel: 3D view of first order electric field near the neutron star (Lyutikov 2023). The central sphere is the neutron star. The blue surface is the magnetic field flux surface (magnetic field lines lie on the surface pointing in the  $z$  direction). Arrows are electric fields sliced at  $x = 0, y = 0, z = 0$ . In the frame of the neutron star plasma is moving in the  $+x$  direction. Bounded ear-like surfaces are regions where  $\beta_{EM}$  becomes larger than 1. Right Panel: 2D PIC simulations of relativistic magnetic draping, different orientations of the magnetic field (in the plane and out of the plane). Plotted is plasma density. Dissipative regions downstream, due to magnetic draping, are clearly seen (Cortes+, in prep.)

relative phases of the spin and orbital motions. In the case of merging magnetized neutron stars, if one of the stars is a millisecond pulsar, spinning at  $\sim 10$  msec, the global resonance  $\omega_1 + \omega_2 = 2\Omega$  (spin-plus beat is two times the orbital period) occurs approximately a second before the merger; the total energy of the flare can be as large as 10% of the total magnetic energy, producing bursts of luminosity  $\sim 10^{44}$  erg  $s^{-1}$ . Higher order local resonances may have similar powers, since the amount of involved magnetic flux tubes may be comparable to the total connected flux.

The 2:1 resonance occurs at time

$$t_{1-2} = (-t_m) = 10^{-3} \frac{c^5 (M_1 + M_2)^{1/3}}{G^{5/3} M_1 M_2 \omega^{8/3}} = 5 \times 10^5 P_s^{8/3} \text{ sec}, \quad (6)$$

where  $P_s = 2\pi/\omega$  is the sum-beat (addition) period of the NS spin's,  $M_1$  and  $M_2$  are masses of neutron stars (assumed to be equal to  $1.4M_\odot$ ). Thus, the most interesting case is one of the neutron star is a recycled millisecond pulsar. For example, if  $P_s = 10$  msec, then  $(-t_m) = 2$  sec. At that moment stars are separated by

$$r = (G(M_1 + M_2))^{1/3} \Omega^{-2/3} \approx 10^7 \text{ cm}, \quad (7)$$

approximately ten times the radius.

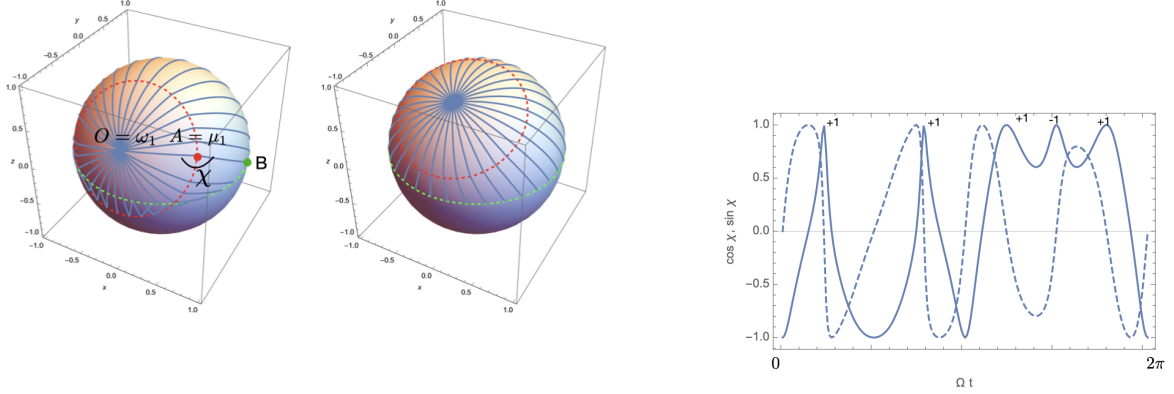


Fig. 4.— Left panels: Twisting of coupled magnetospheres. The sphere represents a space of the directions of the magnetic field. Red dashed circle is the trajectory of the direction of the magnetic field at point  $A$  (direction of magnetic moment of 1); it rotates with the angular frequency  $\omega_A = \omega_1$  around point  $O$ , the direction of the spin of the first star. For both plots  $\omega_1 = \Omega$ : one spin per one full orbital rotation. Left panel inclination  $\theta_A = \pi/3$ , right panel  $\theta_A = \pi/6$  (these are the angles between orbital momentum  $\vec{\Omega}$  and the spin  $\vec{\omega}_1$ ). Radius of the circle  $\theta_{A,c} = \pi/4$  (this is the angle between the spin  $\vec{\omega}_1$  and the magnetic field  $\vec{\mu}_1$ ). Notice how arcs cross-over in the lower part in the left panel, when point  $A$  is below the equator. Right panel: Counting the twist. Plotted is the angle  $\chi$ , spin of  $A$  - magnetic moment of  $A$  - direction to  $B$ , ( $\cos \chi$  - solid line,  $\sin \chi$  - dashed line). One twist is added to magnetic stripe connecting two stars when  $\cos \chi = 1$  and  $\sin \chi$  changes from positive to negative; one rotation is subtracted when  $\sin \chi$  changes from negative to positive. In this example  $\omega_A = 5\Omega$ ,  $\theta_A = \pi/3$  and  $\theta_{A,c} = \pi/4$  (Cherkis and Lyutikov 2021).

We can also estimate how flaring will evolve with time. At exact resonance there is no shear, no flaring. As the orbit shrinks, the system gets out of the resonance, field lines are becoming twisted. Assuming that flares occur after a fixed twist angle  $\sim 1$ , the time between flares evaluates to

$$t_f = \frac{4P}{3\pi} \frac{t_{1-2}}{t - t_{1-2}} \quad (8)$$

In addition to 2:1 global resonance, there are many other possible resonances of the type  $m(\omega_1 + \omega_2) = n\Omega$ . Higher order resonances involves only those magnetic lines whose direction at the star surface lie in both the interacting magnetic polar cap and in the resonant region.

A flare may release an amount of energy contained within the flux tube connecting two stars on reconnection time scale: the light time travel over the orbital separation,  $\sim r/c$ , see Fig. 5. The

corresponding energies  $E_f$  and luminosities  $L_f$  of the resulting flares estimate to (upper limits)

$$\begin{aligned}
 E_f &\sim B_{NS}^2 \frac{R_{NS}^6}{r^3} = 10^{39} \left( \frac{-t}{\text{sec}} \right)^{-3/4} \text{ erg} \leq 2 \times 10^{41} \text{ erg} \\
 L_t &\sim \frac{E_f}{r/c} = 10^{42} \left( \frac{-t}{\text{sec}} \right)^{-1} \text{ erg s}^{-1} \leq 10^{45} \text{ erg s}^{-1}
 \end{aligned}
 \tag{9}$$

(upper limits are for  $-t = 10^{-3}$  seconds). (see also Most and Philippov 2022).

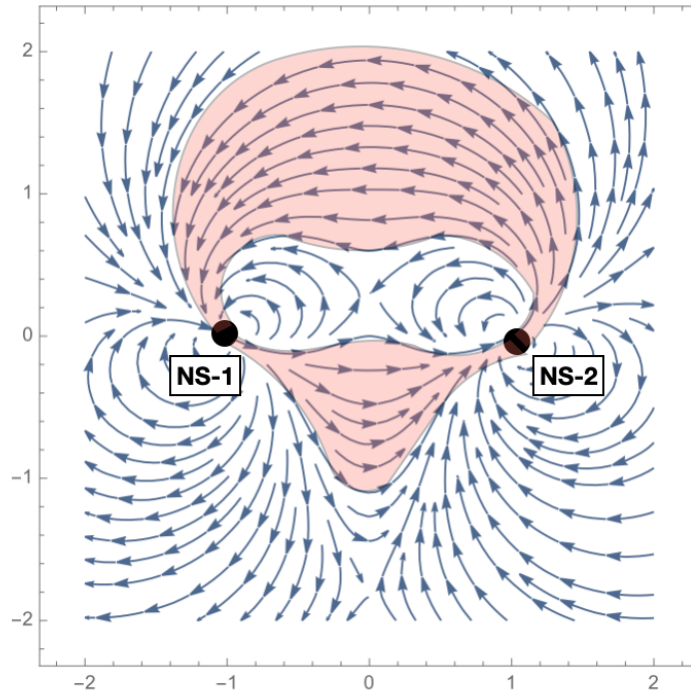


Fig. 5.— Example of coupled neutron stars magnetospheres. The highlighted region contains field lines connecting two stars. Under certain conditions (Cherkis and Lyutikov 2021) the magnetic field lines in the coupled region are slowly twisted, reach an instability point, and release magnetic energy on light travel time  $\sim r/c$ .

#### 2.4. Magnetic field evolution during NS to BH collapse

During the merger of neutron stars, a transient, super-massive, fast-rotating neutron star is formed (Rezzolla et al. 2011). After 10-100 milliseconds it collapses into a black hole. What are the possible observational effects of this collapse?

Importantly: the magnetic energy contained within the collapsing neutron star magnetosphere *is not* released an electromagnetic impulse during formation of a black hole, as would be predicted by the No-Hair theorem, Fig. 6. There is no EM pulse contemporaneous with the NS to BH



collapse (Lyutikov 2011b). The collapse of a NS into the BH happens smoothly, without natural formation of current sheets or other dissipative structures on the open field lines and, thus, does not allow the magnetic field to become disconnected from the star and escape to infinity. As long as an isolated Kerr black hole can produce plasma and currents, it does not lose its open magnetic field lines, its magnetospheric structure evolved towards a split monopole and the black hole spins down electromagnetically (the closed field lines get absorbed by the hole).

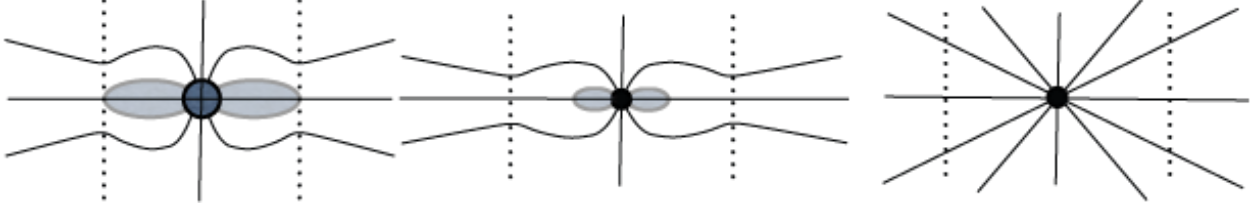


Fig. 6.— Cartoon of the structure of magnetic fields around a collapsing rotating neutron star. Initially, left panel, the magnetic field is that of an isolated pulsar, with a set of field lines closing within the light cylinder (dashed vertical lines). Immediately after the collapse, central panel, the structure is similar. The closed field lines are absorbed by the black hole, while the open field lines remain attached to the black hole; the system relaxes to the monopole structure (right panel), Lyutikov (2011b)

To prove this point (Lyutikov 2011b) generalized the Michel’s solution of monopolar magnetospheres (Michel 1973) to arbitrary  $\Omega(r_{\text{fast}} - t)$  in General relativity. The argument of  $\Omega$  should be evaluated at the position of a radially propagating fast mode in the Schwarzschild metric with  $dr_{\text{fast}}/dt = \alpha^2$ , Fig. 7

- Analytically: time-dependent B-field in Schwarzschild geom.

$$B_\phi = -\frac{R_s^2 \Omega \sin \theta}{\alpha r} B_s, \quad B_r = \left(\frac{R_s}{r}\right)^2 B_s,$$

$$E_\theta = B_\phi, \quad j_r = -2 \left(\frac{R_s}{r}\right)^2 \frac{\cos \theta \Omega B_s}{\alpha}$$

$$\Omega \equiv \Omega (r - t + r(1 - \alpha^2) \ln(r\alpha^2)) \quad \alpha = \sqrt{1 - 2M/r}$$

- Nonlinear, time-dependent solution in GR (small  $\alpha$ )

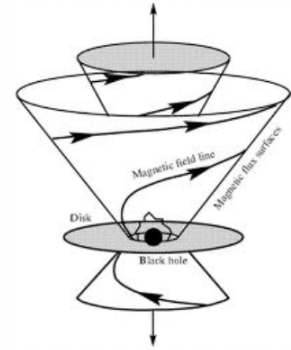


Fig. 7.— Evolution of magnetic field during NS  $\rightarrow$  BH collapse (Lyutikov 2011b). Analytical solution for split-monopole magnetosphere demonstrates that open field lines are not “cut out” during collapse.

It follows, that the No-Hair theorem is not formally applicable for black holes formed from collapse of a rotating neutron star. Rotating neutron stars can self-produce particles via vacuum

breakdown forming a highly conducting plasma magnetosphere such that magnetic field lines are effectively “frozen-in” the star both before and during collapse. In the limit of no resistivity, this introduces a topological constraint which prohibits the magnetic field from sliding off the newly-formed event horizon. As a result, during collapse of a neutron star into a black hole, the latter conserves the number of magnetic flux tubes, hair. Hair can be counted (!)

$$N_B = e\Phi_\infty/(\pi c\hbar) = B_{NS}eR_{NS}^3\Omega_{NS}/(c^2\hbar) = 10^{41} \frac{B_{NS}}{10^{12}\text{G}} \frac{P_{NS}}{1\text{msec}}.$$

$$\Phi_\infty \approx \pi B_{NS}R_{NS}^3\Omega_{NS}/c \tag{10}$$

$\Phi_\infty$  is the initial magnetic flux through the hemispheres of the progenitor and out to infinity, and  $\Omega_{NS} = 2\pi/P_{NS}$  is pre-collapse spin of the neutron star.

This theoretical result was tested by Lyutikov and McKinney (2011) (see also latest simulations by Bransgrove et al. 2021; Most and Philippov 2023), Fig. 8, via three-dimensional general relativistic plasma simulations of rotating black holes that start with a neutron star dipole magnetic field with no currents initially present outside the event horizon. The black hole’s magnetosphere subsequently relaxes to the split monopole magnetic field geometry with self-generated currents outside the event horizon. The dissipation of the resulting equatorial current sheet leads to a slow loss of the anchored flux tubes, a process that balds the black hole on long resistive time scales rather than the short light-crossing time scales expected from the vacuum “no-hair” theorem. Eventually, reconnection events will lead to magnetic field release (*Slowly balding black holes*, Lyutikov and McKinney 2011; Most and Philippov 2023), shutting down the electromagnetic BH engine forever.

The power produced by the resulting isolated BH (we stress - *isolated* - with magnetic field not supported by accretion, but anchored in the BH horizon by the ideal condition of the surrounding plasma) is

$$L_h \sim \Phi_\infty^2\Omega^2/c = 6 \times 10^{44} \text{ erg s}^{-1} \tag{11}$$

The estimate of (11) is for magnetic field of  $10^{12}$  G. Power  $L_h$  can be substantial, especially if magnetic field is amplified by turbulence resulting from shear instabilities during the merger (Giacomazzo et al. 2015). For example, for quantum magnetic field and BH spin of 1 msec, the resulting “hair-powered” BH emission can be as high as  $L_h \sim 3 \times 10^{48} \text{ erg s}^{-1}$ . Such process may contribute to the production of prompt emission in short GRBs (Lyutikov 2013).

The post-collapse (magnetic) “hair-driven” stage is limited by how fast (or how slow) magnetic field slides off the BH due to resistive effects in the equatorial current sheet. Numerical estimates (Lyutikov and McKinney 2011; Most and Philippov 2023) indicate relatively rapid “hair loss” (still on time scales much longer than the dynamics time scale predicted by the No-Hair theorem. But resistive effects in numerical simulations are typically larger than physically expected.

### 3. Magnetospheric interaction in BH-NS mergers

The Blandford and Znajek (1977) paradigm outlines how the energy of a rotating black hole can be extracted to generate jets and the observed broadband emission. There is another possibility: Schwarzschild black holes as unipolar inductors (Lyutikov 2011a; Morozova et al. 2014).

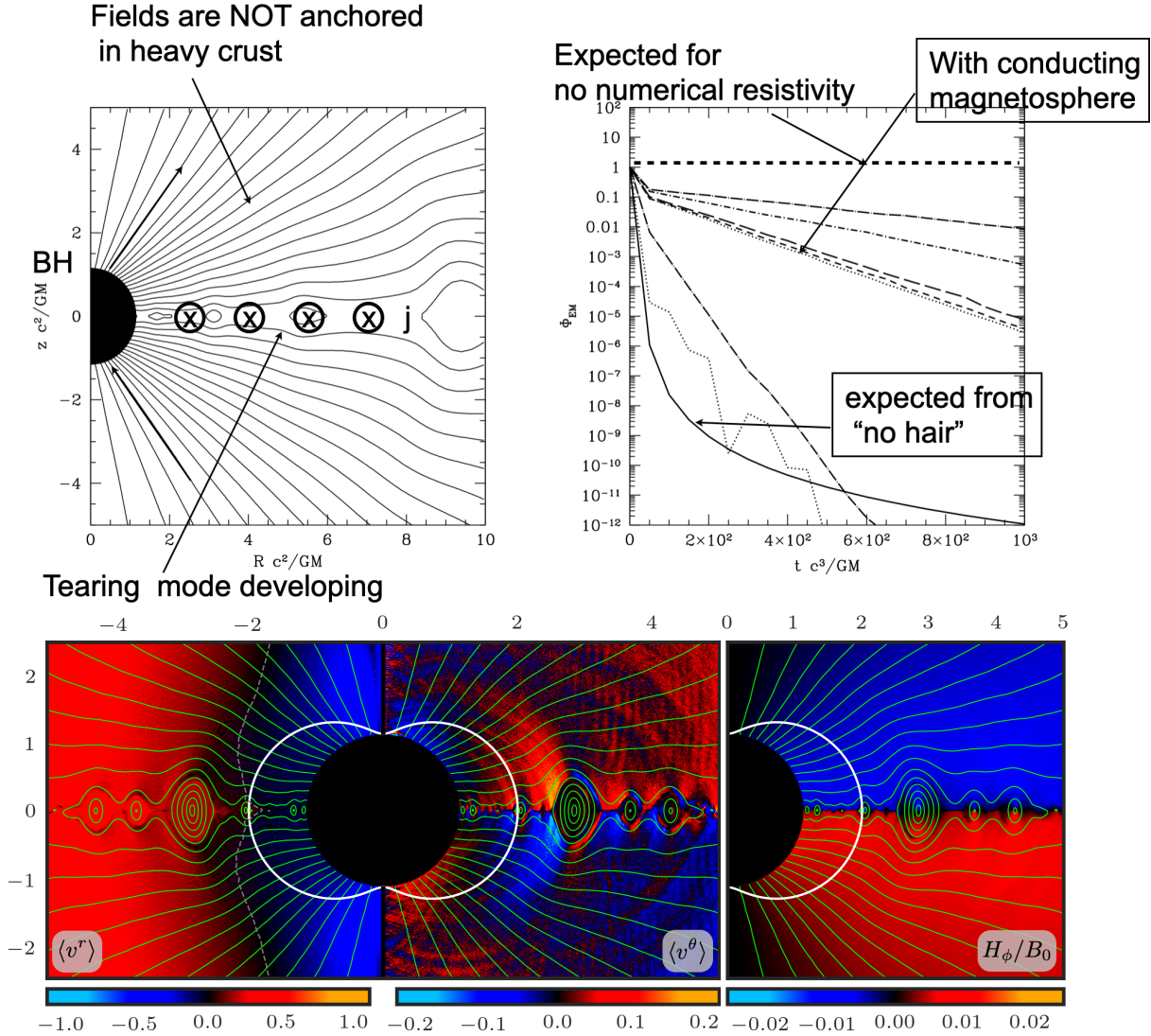


Fig. 8.— Magnetic hair of newly formed BH, numerical simulations. Top: Lyutikov and McKinney (2011), annotated; bottom: Bransgrove et al. (2021), zoomed-in view of the equatorial reconnection current sheet.

Two related processes are expected to be at play. First, the motion of a Schwarzschild black hole through a constant magnetic field  $B_0$  in vacuum induces a component of the electric field along the magnetic field,  $\mathbf{E} \cdot \mathbf{B} \neq 0$ . Another breakdown of the ideal condition is the creation of regions where electric field becomes larger than magnetic field, Fig. 9.

Regions of  $\mathbf{E} \cdot \mathbf{B} \neq 0$  and  $E > B$  will lead to dissipation via radiative effects and vacuum breakdown. To bring the system “back to normal”, an electric charge density will be produced, of the order of  $\rho_{\text{ind}} = B_0 \beta_0 / (2\pi e R_G)$ , where  $R_G = 2GM/c^2$  is the Schwarzschild radius and  $M$  is mass of the black hole; the charge density  $\rho_{\text{ind}}$  is similar to the Goldreich-Julian density.

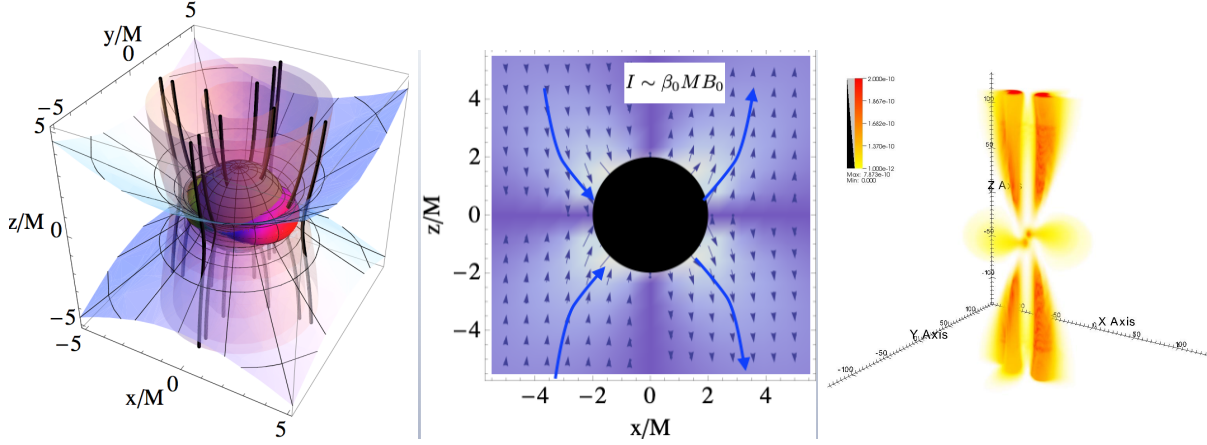


Fig. 9.— Left and center panels: 3D view of the magnetosphere of a black hole moving linearly through magnetic field (after Lyutikov 2011a). A BH generate *quadruple* current flow. Right panel: GR-MHD simulations of merging black holes in external magnetic field by Palenzuela et al. (2010). (We point out that the corresponding PIC simulations have not been done so far.)

As a result, the magnetospheres of moving black holes resemble in many respects the magnetospheres of rotationally-powered pulsars, with pair formation fronts and outer gaps, where the sign of the induced charge changes. The black hole generates bipolar electromagnetic jets each consisting of two counter-aligned current flows (four current flows total), each carrying an electric current of the order  $I \approx eB_0 R_G \beta_0$ , Fig. 9. The electromagnetic power of the jets is  $L \approx (GM)^2 B_0^2 \beta_0^2 / c^3$  (Lyutikov 2011a; Most and Philippov 2023).

Since the resulting electrodynamics is in many respects similar to pulsars, merging black holes may generate coherent radio and high-energy emission beamed approximately along the orbital normal (Lyutikov 2011a; Most and Philippov 2023).

For black hole moving linearly through magnetic field, the relations (1) gives (assuming orbital motion is dominated by the BH)

$$L_{BH-NS} = \frac{(GM_{BH})^3 B_{NS}^2}{\pi c^5 R_{NS}} \left( \frac{R_{NS}}{r} \right)^7 = \begin{cases} 3 \times 10^{46} \text{ erg s}^{-1} m_1^3 \left( \frac{R_{NS}}{r} \right)^7 \\ 5 \times 10^{35} \text{ erg s}^{-1} m_1^{-1/2} \left( \frac{-t}{\text{sec}} \right)^{-7/4}, \end{cases}$$

$$m_1 = \log_{10} \frac{M_{BH}}{M_{\odot}} \geq 1 \tag{12}$$

#### 4. Observation strategy

Realistically, it's a huge challenge to detect precursor emission to LVK sources. Yet the possible information to be gained - detailed properties of the merging objects - would be highly valuable to constraint the physical properties of the compacts, and by extension the larger astronomical picture of evolution of stellar remnants. As we discuss next, some (less likely) channels are already in places, some will require dedicated observing strategy. Yet the corresponding costs - *e.g.*, numerically

targeting large-view radio phased array telescopes - are comparatively mild.

#### 4.1. Best chance: low frequency radio

The best chance of seeing precursor emission is the production of coherent pulsar-like radio emission (Hansen and Lyutikov 2001; Lyutikov 2019; Cooper et al. 2023). For example, if peak power is emitted in radio with efficiency  $\eta_R = 10^{-3}\eta_{R,-3}$ , the expected observed flux may be in the Jansky range:

$$F_{\nu,peak} = 0.5 \text{ Jy} \eta_{R,-3} \nu_9^{-1} d_{200}^{-2} \quad (13)$$

where  $\nu = 10^9 \nu_9$  Hz is the observed frequency and  $d_{200} = d/(200)$  Mpc is distance to the source. Thus, in the best case scenarios the radio power can be substantial.

In addition to LVK early warnings alerts (Sachdev et al. 2020),  $\sim$  one minute advanced notice, radio pulses have another advantage: they will experience dispersive delay of

$$\Delta t = 14 \text{ sec} \nu_9^{-2} d_{200} \quad (14)$$

(see also Pshirkov and Postnov 2010). At low frequencies,  $\leq 100$  MHz, the delay can be nearly half an hour! (Tian et al. 2023, discussed MWA detectability of LVK precursors). The expected localization of early alerts is of the order of 1000 square degrees. Such relatively wide field requires particular observing mode, similar to the digital beamforming of  $\sim 30$  square degrees used to localize a single FRB

The radio emission is expected to be modulated on the spin period(s) of the merging neutron stars, as well as orbital-spin beats, §2.3. Dispersion measure will be similar to FRBs, in the hundreds. (Mergers were the leading model of FRBs before the Repeater was discovered Spitler et al. 2016, .) Potentially problematic for detection of periodicity is the orbital evolution during last orbits (when emission is most powerful), as the beat frequencies evolve with time. This introduces complication for the de-dispersion process.

#### 4.2. High energy: beaming needed

Isotropic powers (3,5) are not sufficient to be detected by high energy all-sky monitors satellites. Unknown location does not allow use of more sensitive targeted instruments. Early alerts of  $\leq$  a minute are too short to slew. The SWIFTGUANO (Tohuvavohu et al. 2020) pipeline will be able to keep the data, yet the satellite won't slew.

There are possible exceptions, though. Emission produced in  $\mathbf{E} \cdot \mathbf{B} \neq 0$  gaps will be beamed along the local magnetic field. Beamed emission reduces chances of been seen, but increases the flux. Both NS-NS and NS-BH mergers are expected to produce beamed emission.

### 4.3. Optical

Survey optical telescopes typically have fields of ten(s) square degrees. They are unlikely to be just looking at the right direction. LIGO early alerts open a possibility.

Optical flash of  $\sim 10^{43}$  erg  $s^{-1}$  coming from 200 Mpc would correspond to apparent magnitude of  $m \sim 15$ , but only for a millisecond (see a closely related discussion of FRB optical detectability Lyutikov and Lorimer 2016). Fast read-out is the key then. If the readout time is ten seconds, a millisecond flash will give a fluence  $\approx 10^4$  times smaller resulting in an image 10 magnitudes fainter,  $m \sim 25$ . This is somewhat below Zwicky Transient Facility (ZTF, Graham et al. 2019; Bellm et al. 2019).

ASAS-SN (Holoiien et al. 2016), EVRYSCOPE (Law et al. 2015), DECam (Schlafly et al. 2018), ATLAS (Tonry et al. 2018), Pan-STARRS (Kaiser et al. 2002) seem to be below the required threshold. (DECam is the most sensitive of them all, but has the field of view of "only" 3 deg. sq.). The Argus Array ("Evrscope on steroids" Law et al. 2022) is highly promising.

The forthcoming Large Synoptic Survey Telescope (LSST; Ivezić et al. 2008) is expected to fare better. It will also have large field of view, almost 10 square degrees, and will be able to reach magnitude  $m = 25$  within two exposures of  $\sim 15$  s each.

The analysis of LSST data would be problematic, though: the image will be only on one plate, close to the limit of LSST sensitivity. But there are a lot of optical transients (*e.g.*, asteroids passing by), so that single-image sources are typically discarded.

An important fast readout procedure, the Readout While Exposing mode (RWE, Bianco et al. 2009), is been tested on wide-field instruments, like Megacam (Bianco et al. 2009) and ZTF (Andreoni et al., in prep). It is expected to reach a few milliseconds readout rate (at the expense of sacrificing one dimension in the image). Some preliminary testing is going on (Phinney *et al.*, priv. comm.). It is not planned to be implemented at LSST, though.

Another possibly interesting optical wide-field \*and\* fast read-out observatory is Tomo-e Gozen (Sako et al. 2018; Richmond et al. 2020; Oshikiri et al. 2024) telescope, with 10-500ms time resolution.

## 5. Supermassive BH-BH mergers and LISA precursors

Merger of supermassive BHs - target of future LISA observations - may also produce precursor emission (Palenzuela et al. 2010; Lyutikov 2011a). The difference from the NS-BH merger is that the magnetic field needs to be supplied by the external accretion disk. In addition, accretion contribution - as opposed to the purely electromagnetic discussed here - may be considerable (Milosavljević and Phinney 2005; Cuadra et al. 2009; Bartos et al. 2017). As the EM power is concerned, in Eq. (1) the magnetic field is then parametrized by the properties of the accretion disk (*e.g.*, mass accretion rate,  $\alpha$ -viscosity, and location of the inner edge), while the velocity if the Keplerian velocity of the merging BHs.

The power of unipolar induction, for a given external magnetic field, remains mild. For exam-

ple, comparing the power of the Schwarzschild black hole as unipolar inductor, with the Blandford-Znajek power in a given magnetic field,  $L_{BZ} \sim a^2 B^2 M^2$  ( $a$  is the black hole spin parameter), gives

$$\frac{L_{EM}}{L_{BZ}} \approx \frac{\beta_K^2}{a^2} \quad (15)$$

( $\beta_K$  is dimensionless Keplerian velocity. For fast rotating black holes,  $a \sim 1$ , the power of the unipolar inductor is subdominant until right before the merger.

In addition, merging supermassive BHs may produce plerionic-type emission Lyutikov (2011a). Most of the EM power will leave the black holes' region in a form of relativistic highly magnetized wind. Even though the instantaneous power is typically much smaller than the Eddington power corresponding to masses  $M$ , the total released energy can be substantial.

An important, and uncertain, parameter is the decoupling radius, when the gravitational radiation acts faster on the BH separation than the accretion time scale of the inner disk. Overall, one can expect  $\sim 10^{47} \text{ erg } m_6^{9/5}$  ergs deposited (see Lyutikov 2011a, for estimates).

The Nanograv connection. Evidence for a low-frequency stochastic gravitational-wave background has recently been reported by *Nanograv* based on analyses of pulsar timing array data (Agazie et al. 2023a). The most likely source of such a background is a population of supermassive black hole binaries, the loudest of which may be individually detected in these data sets (Agazie et al. 2023b). Two candidate sources showed marginal/weak evidence of detection.

Objectively, in radio, observations of electromagnetic from supermassive binary black holes merger is a difficult task due to long periods (years) and poor localization even if a particular single source can be identified. In radio, it is hard to control for all the systematics over the years.

LSST may offer a better coverage: it is expected that after 5 years of LSST observations, tens of true binaries will be detectable, as periodically variable AGNe (Kelley et al. 2019a,b). Given the period from Nanograv and LSST coverage, one may expect/hope to identify electromagnetic signatures of merging black hole.

## 6. In conclusion

Realistically, detecting precursor emission to LVK sources is highly challenging, yet the corresponding costs in X-ray and radio - numerically targeting large-view radio phased array telescopes, and SWIFTGUANO - are comparatively mild. Optical detections are the most challenging.

## 7. Disclaimer and Acknowledgment

These notes are not intended as a review of the field, or formal publication. Future discussions/collaborations are encouraged.

I would like to thank Igor Andreoni for most enlightening discussions. I also thank Shri Kulkarni, Elias Most and Sterl Phinney for comments.

## REFERENCES

- S. Sachdev, R. Magee, C. Hanna, K. Cannon, L. Singer, J. R. SK, D. Mukherjee, S. Caudill, C. Chan, J. D. E. Creighton, et al., *ApJ* **905**, L25 (2020), 2008.04288.
- F. Foucart, T. Hinderer, and S. Nissanke, *Phys. Rev. D* **98**, 081501 (2018), 1807.00011.
- E. Nakar, *Phys. Rep.* **886**, 1 (2020), 1912.05659.
- R. D. Blandford, in *Lighthouses of the Universe: The Most Luminous Celestial Objects and Their Use for Cosmology*, edited by M. Gilfanov, R. Sunyeav, and E. Churazov (2002), p. 381, astro-ph/0202265.
- P. Goldreich and W. H. Julian, *ApJ* **157**, 869 (1969).
- P. Goldreich and D. Lynden-Bell, *ApJ* **156**, 59 (1969).
- M. Lyutikov, *Phys. Rev. D* **83**, 064001 (2011a), 1101.0639.
- B. M. S. Hansen and M. Lyutikov, *MNRAS* **322**, 695 (2001), astro-ph/0003218.
- E. R. Most and A. A. Philippov, *ApJ* **956**, L33 (2023), 2309.04271.
- M. Lyutikov, *MNRAS* **483**, 2766 (2019).
- E. R. Most and A. A. Philippov, *MNRAS* **515**, 2710 (2022), 2205.09643.
- M. Lyutikov, *Phys. Rev. E* **107**, 025205 (2023), 2211.14433.
- I. H. Cairns, in *Physics of the Outer Heliosphere*, edited by V. Florinski, N. V. Pogorelov, and G. P. Zank (2004), vol. 719 of *American Institute of Physics Conference Series*, pp. 381–386.
- M. Lyutikov, *MNRAS* **373**, 73 (2006), astro-ph/0604178.
- L. J. Dursi and C. Pfrommer, *ApJ* **677**, 993 (2008), 0711.0213.
- S. A. Cherkis and M. Lyutikov, *ApJ* **923**, 13 (2021), 2107.09702.
- L. Rezzolla, B. Giacomazzo, L. Baiotti, J. Granot, C. Kouveliotou, and M. A. Aloy, *ApJ* **732**, L6 (2011), 1101.4298.
- M. Lyutikov, *Phys. Rev. D* **83**, 124035 (2011b), 1104.1091.
- F. C. Michel, *ApJ* **180**, L133 (1973).
- M. Lyutikov and J. C. McKinney, *Phys. Rev. D* **84**, 084019 (2011), 1109.0584.
- A. Bransgrove, B. Ripperda, and A. Philippov, *Phys. Rev. Lett.* **127**, 055101 (2021), 2109.14620.
- B. Giacomazzo, J. Zrake, P. C. Duffell, A. I. MacFadyen, and R. Perna, *ApJ* **809**, 39 (2015), 1410.0013.
- M. Lyutikov, *ApJ* **768**, 63 (2013), 1202.6026.



- R. D. Blandford and R. L. Znajek, *MNRAS* **179**, 433 (1977).
- V. S. Morozova, L. Rezzolla, and B. J. Ahmedov, *Phys. Rev. D* **89**, 104030 (2014), 1310.3575.
- C. Palenzuela, L. Lehner, and S. L. Liebling, *Science* **329**, 927 (2010), 1005.1067.
- A. J. Cooper, O. Gupta, Z. Wadiasingh, R. A. M. J. Wijers, O. M. Boersma, I. Andreoni, A. Rowlinson, and K. Gourdji, *MNRAS* **519**, 3923 (2023), 2210.17205.
- M. S. Pshirkov and K. A. Postnov, *Ap&SS* **330**, 13 (2010), 1004.5115.
- J. Tian, G. E. Anderson, A. J. Cooper, K. Gourdji, M. Sokolowski, A. Rowlinson, A. Williams, G. Sleap, D. Dobie, D. L. Kaplan, et al., *PASA* **40**, e050 (2023), 2309.16383.
- L. G. Spitler, P. Scholz, J. W. T. Hessels, S. Bogdanov, A. Brazier, F. Camilo, S. Chatterjee, J. M. Cordes, F. Crawford, J. Deneva, et al., *Nature* **531**, 202 (2016), 1603.00581.
- A. Tohuvavohu, J. A. Kennea, J. DeLaunay, D. M. Palmer, S. B. Cenko, and S. Barthelmy, *ApJ* **900**, 35 (2020), 2005.01751.
- M. Lyutikov and D. R. Lorimer, *ApJ* **824**, L18 (2016), 1605.01468.
- M. J. Graham, S. R. Kulkarni, E. C. Bellm, S. M. Adams, C. Barbarino, N. Blagorodnova, D. Bode-wits, B. Bolin, P. R. Brady, S. B. Cenko, et al., *PASP* **131**, 078001 (2019), 1902.01945.
- E. C. Bellm, S. R. Kulkarni, M. J. Graham, R. Dekany, R. M. Smith, R. Riddle, F. J. Masci, G. Helou, T. A. Prince, S. M. Adams, et al., *PASP* **131**, 018002 (2019), 1902.01932.
- T. W.-S. Holoiën, K. Z. Stanek, C. S. Kochanek, B. J. Shappee, J. L. Prieto, J. Brimacombe, D. Bersier, D. W. Bishop, S. Dong, J. S. Brown, et al., *ArXiv e-prints* (2016), 1604.00396.
- N. M. Law, O. Fors, J. Ratzloff, P. Wulfken, D. Kavanaugh, D. J. Sitar, Z. Pruett, M. N. Birchard, B. N. Barlow, K. Cannon, et al., *PASP* **127**, 234 (2015), 1501.03162.
- E. F. Schlafly, G. M. Green, D. Lang, T. Daylan, D. P. Finkbeiner, A. Lee, A. M. Meisner, D. Schlegel, and F. Valdes, *ApJS* **234**, 39 (2018), 1710.01309.
- J. L. Tonry, L. Denneau, A. N. Heinze, B. Stalder, K. W. Smith, S. J. Smartt, C. W. Stubbs, H. J. Weiland, and A. Rest, *PASP* **130**, 064505 (2018), 1802.00879.
- N. Kaiser, H. Aussel, B. E. Burke, H. Boesgaard, K. Chambers, M. R. Chun, J. N. Heasley, K.-W. Hodapp, B. Hunt, R. Jedicke, et al., in *Survey and Other Telescope Technologies and Discoveries*, edited by J. A. Tyson and S. Wolff (2002), vol. 4836 of *Society of Photo-Optical Instrumentation Engineers (SPIE) Conference Series*, pp. 154–164.
- N. M. Law, H. Corbett, N. W. Gallier, R. Gonzalez, A. Vasquez, G. Walters, L. Machia, J. Ratzloff, K. Ackley, C. Bizon, et al., *PASP* **134**, 035003 (2022), 2107.00664.
- Z. Ivezić, J. A. Tyson, B. Abel, E. Acosta, R. Allsman, Y. AlSayyad, S. F. Anderson, J. Andrew, R. Angel, G. Angeli, et al., *ArXiv e-prints* (2008), 0805.2366.

- F. B. Bianco, P. Protopapas, B. A. McLeod, C. R. Alcock, M. J. Holman, and M. J. Lehner, *AJ* **138**, 568 (2009), 0903.3036.
- S. Sako, R. Ohsawa, H. Takahashi, Y. Kojima, M. Doi, N. Kobayashi, T. Aoki, N. Arima, K. Arimatsu, M. Ichiki, et al., in *Ground-based and Airborne Instrumentation for Astronomy VII*, edited by C. J. Evans, L. Simard, and H. Takami (2018), vol. 10702 of *Society of Photo-Optical Instrumentation Engineers (SPIE) Conference Series*, p. 107020J.
- M. W. Richmond, M. Tanaka, T. Morokuma, S. Sako, R. Ohsawa, N. Arima, N. Tominaga, M. Doi, T. Aoki, K. Arimatsu, et al., *PASJ* **72**, 3 (2020), 1910.11343.
- K. Oshikiri, M. Tanaka, N. Tominaga, T. Morokuma, I. Takahashi, Y. Tambo, H. Hamidani, N. Arima, K. Arimatsu, T. Kasuga, et al., *MNRAS* **527**, 334 (2024), 2310.10066.
- M. Milosavljević and E. S. Phinney, *ApJ* **622**, L93 (2005), astro-ph/0410343.
- J. Cuadra, P. J. Armitage, R. D. Alexander, and M. C. Begelman, *MNRAS* **393**, 1423 (2009), 0809.0311.
- I. Bartos, B. Kocsis, Z. Haiman, and S. Márka, *ApJ* **835**, 165 (2017), 1602.03831.
- G. Agazie, A. Anumalapudi, A. M. Archibald, Z. Arzoumanian, P. T. Baker, B. Bécsy, L. Blecha, A. Brazier, P. R. Brook, S. Burke-Spolaor, et al., *ApJ* **951**, L8 (2023a), 2306.16213.
- G. Agazie, A. Anumalapudi, A. M. Archibald, Z. Arzoumanian, P. T. Baker, B. Bécsy, L. Blecha, A. Brazier, P. R. Brook, S. Burke-Spolaor, et al., *ApJ* **951**, L50 (2023b), 2306.16222.
- L. Kelley, M. Charisi, S. Burke-Spolaor, J. Simon, L. Blecha, T. Bogdanovic, M. Colpi, J. Comerford, D. D’Orazio, M. Dotti, et al., *BAAS* **51**, 490 (2019a), 1903.07644.
- L. Z. Kelley, Z. Haiman, A. Sesana, and L. Hernquist, *MNRAS* **485**, 1579 (2019b), 1809.02138.